Chiral and nonchiral edge states in quantum Hall systems with charge density modulation

Paweł Szumniak,[1,2] Jelena Klinovaja,[1] and Daniel Loss[1]

[1]*Department of Physics, University of Basel, Klingelbergstrasse 82, 4056 Basel, Switzerland*

[2]*AGH University of Science and Technology, Faculty of Physics and Applied Computer Science, al. Mickiewicza 30, 30-059 Kraków, Poland*

(Received 17 December 2015; revised manuscript received 8 June 2016; published 27 June 2016)

We consider a system of weakly coupled wires with quantum Hall effect (QHE) and in the presence of a spatially periodic modulation of the chemical potential along the wire, equivalent to a charge density wave (CDW). We investigate the competition between the two effects which both open a gap. We show that by changing the ratio between the amplitudes of the CDW modulation and the tunneling between wires, one can switch between nontopological CDW-dominated phase to topological QHE-dominated phase. Both phases host edge states of chiral and nonchiral nature robust to on-site disorder. However, only in the topological phase, the edge states are immune to disorder in the phase shifts of the CDWs. We provide analytical solutions for filling factor $\nu = 1$ and study numerically effects of disorder as well as present numerical results for higher filling factors.

DOI: 10.1103/PhysRevB.93.245308

I. INTRODUCTION

Over the past decades topological states of matter attracted a lot of attention both theoretically and experimentally. The striking stability of the quantum Hall effect (QHE) [1,2] can be linked to topology [3]. The time-reversal invariant cousins of the QHE are the two-dimensional (2D) topological insulators (TIs) for which many candidate materials were found or synthesized in recent years [4]. However, despite great progress, the conductance quantization in TI materials is still not as perfect as in the QHE. Thus the experimental focus has shifted in recent years to a more direct study of the edge state physics in TIs, for instance, via Fraunhofer patterns [5,6] and SQUID probes [7,8]. However, the edge states, especially in clean samples, could also be of nontopological origin, for example, due to Tamm-Shockley states [9–11].

Recently, edge state behavior was observed in 2D GaSb heterostructures, but in a regime that is believed to be nontopological, and thus challenging the standard interpretation of this system as a TI [12]. The origin of this unexpected observation is still unclear but it raises the intriguing question whether edge states could not occur in both phases, in the topological as well as in the trivial one, but with different signatures such as, e.g., being helical (chiral) in one phase versus nonhelical (nonchiral) in the other. In other words, the system could host topological edge states for one set of parameters while there exist nontopological edge states for another one. It is thus of fundamental interest to see if realistic models can be constructed which demonstrate that, in principle, these two scenarios do not need to exclude each other.

In the present work, we propose a system related to the QHE regime where exactly such a mixed behavior of edge state physics can emerge. The system we consider is given by a 2D array of tunnel coupled wires in the presence of a magnetic field and charge density waves (CDWs) inside the wires. This provides two different mechanisms (QHE and CDW) for inducing gaps and edge states which can compete with each other. Such CDWs may be induced intrinsically by electron-electron interactions [13–15], extrinsically by periodically arranged gates inducing spatial modulations of the chemical potential, or by an internal superlattice structure [16,17]; see Fig. 1. We show that by tuning the ratio between the amplitude of the CDW modulation and the tunneling amplitude between the wires the system undergoes a phase transition between a nontopological (CDW dominated) phase, which supports predominantly nonchiral edge states, and a topological (QHE dominated) phase, which supports predominantly chiral edge states. However, in both phases, one can find both chiral and nonchiral regimes. These results are supported by both numerical and analytical calculations. We confirm numerically that, as expected, the topological chiral states are less susceptible to disorder.

II. THEORETICAL MODEL

A. Lattice tight-binding model

We consider a 2D coupled wire construction [18–27] in the presence of a perpendicular uniform magnetic field; see Fig. 1. We assume that the propagation is anisotropic in the xy plane, mainly for analytical convenience (in Appendix B we show numerically that our results can be extended to isotropic systems). The tunneling amplitude along the wires, aligned in the x direction, is thus larger than the one between the wires in the y direction. This allows us to treat the wires as independent one-dimensional channels only weakly coupled to their neighboring wires. In addition, we include a CDW modulation along the wire. The system is then described by the following tight-binding Hamiltonian,

$$H = \sum_{n,m}(-t c^{\dagger}_{n+1,m}c_{n,m} - t_y e^{in\phi} c^{\dagger}_{n,m+1}c_{n,m} - [U_0\cos(2k_w n a_x + \varphi) + \mu/2]c^{\dagger}_{n,m}c_{n,m} + \text{H.c.}), \quad (1)$$

where $c_{n,m}$ is the annihilation operator acting on the electron at a site (n,m) of the lattice with the lattice constant a_x (a_y) in the x (y) direction. For simplicity we consider spinless electrons in this work. We choose the hopping amplitude along the x direction $t > 0$ to be much larger than the hopping along the y direction $t_y > 0$. The uniform magnetic field applied in the z direction, $\boldsymbol{B} = B\,\boldsymbol{e}_z$, and the corresponding vector potential $\boldsymbol{A} = Bx\,\boldsymbol{e}_y$ is chosen along the y axis, yielding the orbital Peierls phase $\phi = eBa_xa_y/\hbar c$. The chemical potential μ is modulated with the CDW amplitude $2U_0 > 0$ and the period

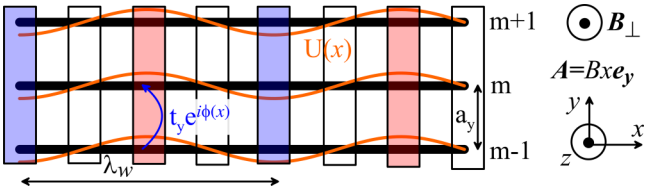

FIG. 1. 2D strip of weakly coupled wires in a perpendicular magnetic field $B_\perp$ applied along the z axis. The wires (thick black lines) aligned along the x axis and labeled by the index m are weakly coupled with tunnel amplitude t_y in the y direction. The vector potential $\mathbf{A} = Bx\,\boldsymbol{e}_y$ is chosen to be in the y direction such that the phase $\phi(x) = eBa_y x/\hbar c$ acquired in the tunneling is position dependent, where a_y is the distance between neighboring wires. There is a CDW modulation $U(x)$ (orange wavy line) of the chemical potential inside the wires, with period λ_w tuned to the Fermi wavelength λ_F.

$\lambda_w = \pi/k_w$. The angle φ is the phase of the CDW at the left edge of the wire ($n = 0$).

With this choice of the vector potential $\mathbf{A}$, the system is translation invariant in the y direction; thus we can introduce the momentum k_y via Fourier transformation $c_{n,m} = \frac{1}{\sqrt{N_y}}\sum_{k_y} c_{n,k_y} e^{-imk_y a_y}$, where N_y is the number of lattice sites in the y direction. The Hamiltonian becomes diagonal in k_y space,

$$H = \sum_{n,k_y}\Big(\big[-tc^\dagger_{n+1,k_y}c_{n,k_y} + \text{H.c.}\big] - c^\dagger_{n,k_y}c_{n,k_y} \times \left[\mu + 2U_0\cos(2k_w n a_x + \varphi) + 2t_y\cos(n\phi + k_y a_y)\right]\Big). \quad (2)$$

As a result, the eigenfunctions of H factorize as $e^{ik_y y}\psi_{k_y}(x)$, with $x = na_x$ and $y = ma_y$. From now on, we focus on $\psi_{k_y}(x)$ and treat k_y as a parameter.

B. Continuum model

To obtain the analytical solution, it is convenient to change to the continuum description [28,29] (see also the SM for details [30]). In this case, the resonant magnetic field leading to $\phi = 2k_F a_x$, corresponds to the filling factor $\nu = 1$ [20]. In the weak tunneling and weak modulation regime, the spectrum can be linearized around the Fermi points, $\pm k_F$, defined via the chemical potential as $k_F a_x = \arccos(-\mu/2t)$. In the regime of interest, the CDW modulation competes with the quantum Hall effect when the period of the CDW is chosen to be resonant, i.e., $k_w = k_F$. The electron operators can be expressed in terms of slowly varying right $[R(x)]$ and left $[L(x)]$ movers as $\Psi(x) = R(x)e^{ik_F x} + L(x)e^{-ik_F x}$. The corresponding Hamiltonian density $\mathcal{H}$, defined via $H = \int dx\,\Psi^\dagger(x)\mathcal{H}\Psi(x)$, can be written in terms of Pauli matrices $\boldsymbol{\sigma}$ acting on the left-right mover subspace $\Psi = (R, L)$ as

$$\mathcal{H} = v_F\hat{p}\sigma_z - [U_0\cos(\varphi) + t_y\cos(k_y a_y)]\sigma_x + [U_0\sin(\varphi) + t_y\sin(k_y a_y)]\sigma_y, \quad (3)$$

where $\hat{p} = -i\hbar\partial_x$ is the momentum operator and the Fermi velocity v_F is given by $\hbar v_F = 2ta_x\sin(k_F a_x)$. The bulk energy spectrum is given by

$$E^2_\pm = (\hbar v_F k)^2 + U_0^2 + t_y^2 + 2t_y U_0\cos(\varphi - k_y a_y) \quad (4)$$

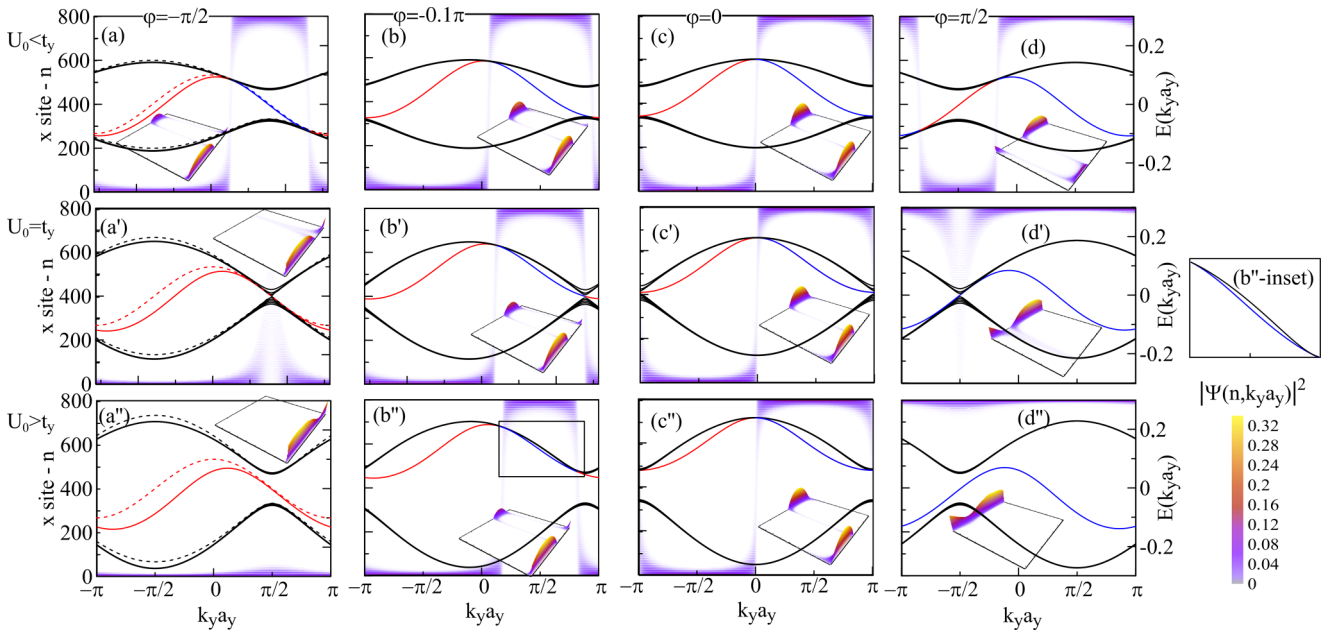

FIG. 2. Energy spectrum $E(k_y a_y)$ near the band gap around the Fermi level defined at $\mu = -\sqrt{2}t$: (a)–(d) in the topological phase ($t_y > U_0 = 0.05t$), (a′)–(d′) at the phase transition point ($t_y = U_0 = 0.1t$), and (a″)–(d″) in the nontopological phase ($t_y < U_0 = 0.15t$) for $\nu = 1$. The panel columns (a), (b), (c), and (d) correspond to the phase shift of the CDW modulation $\varphi = -\pi/2,\ -0.1\pi,\ 0$, and $\pi/2$, respectively. The energy of the edge state and the bulk spectral edge is found both numerically (solid line) and analytically (dashed line), while the color map represents $|\Psi(n,k_y)|^2$ for the edge state wave function probability. The position at site n (energy) is marked on the left (right) axis. We note that edge states can be found both in the topological and nontopological phase. By changing μ, the edge states can be tuned between being chiral and nonchiral independent in both phases; see panels (a) and (b″).

and depends on both k and k_y momenta. Here, E_+ (E_-) corresponds to the part of the spectrum above (below) μ. The size of the bulk gap $2\Delta_g = \min_k(E_+ - E_-)$ for given k_y becomes

$$\Delta_g(k_y) \equiv D = \sqrt{U_0^2 + t_y^2 + 2U_0 t_y \cos(\varphi - k_y a_y)}. \quad (5)$$

We note that the system is gapless if $t_y = U_0$ and $\varphi = k_y a_y + \pi$ but fully gapped otherwise; see Fig. 2. This closing and reopening of the gap hints to a topological phase transition [31]. For a strip of width W, one can thus expect the presence of edge states at the boundaries with energies lying inside the bulk gap. In order to explore the possibility of such edge states we consider a semi-infinite strip ($x \geqslant 0$) and exploit the method developed in Ref. [32]. Furthermore, we assume that W is much larger than the localization length ξ of the edge state [33]. Thus we impose vanishing boundary conditions at the end of the strip $\psi_{k_y}(0) = 0$, which further imposes the constraint $R(0) = -L(0)$. The energy spectrum of the edge state is then found to be

$$\varepsilon(\varphi, k_y) = U_0 \cos(\varphi) + t_y \cos(k_y a_y), \quad (6)$$

under the condition that $U_0 \sin(\varphi) + t_y \sin(k_y a_y) < 0$. The corresponding wave function of the left edge state at energy $\epsilon(\varphi, k_y)$ is given by $\psi_{k_y}(x) \sim \sin(k_F x) e^{-x/\xi}$ with the localization length

$$\xi = -\hbar v_F / |U_0 \sin(\varphi) + t_y \sin(k_y a_y)|. \quad (7)$$

These edge states propagate along the boundaries in y direction. They can be considered as a 1D extension of fractional fermions of the Jackiw-Rebbi type [11,32,34–37].

III. TOPOLOGICAL TRANSITION BETWEEN CDW AND QHE PHASE

There are two important phases the system can be tuned into: the nontopological phase, dominated by the CDW modulation, and the topological QHE phase at filling factor $\nu = 1$ (higher filling factors are discussed in Appendix D), dominated by the magnetic field. We study now the transition between these two phases both analytically and by diagonalizing numerically the tight-binding Hamiltonians; see Eqs. (2) and (3). In the calculations we fix the parameters as follows: $t_y/t = 0.1$ and $k_F = k_w = \pi/4a_x$. The topological transition is induced by changing the amplitude of the CDW U_0 with respect to the tunneling amplitude t_y between wires. We are interested in the bulk band represented by the edge of the gap $\Delta_g(k_y)$ and in the edge state wave function probability $|\psi(n, k_y)|^2$ and its dispersion $\epsilon(k_y a_y)$.

In the topological phase, $t_y > U_0$, the edge state spectrum merges with the bulk gap at two points $\bar{k}_\pm$ (one from the electron band and one from the hole band) determined by the condition $\epsilon(\varphi, \bar{k}_\pm) = \pm\Delta_g(\bar{k}_\pm)$, leading to $\sin(\bar{k}_\pm a_y) = -(U_0/t_y)\sin\varphi$. In other words, for any given value of φ, the edge state exists only for the range of momenta $k_y \in (\bar{k}_-, \bar{k}_+)$; see Figs. 2(a)–2(d). Here, we can further distinguish between two regimes. If $\varphi \in (0, \pi)$ [$\varphi \in (-\pi, 0)$] corresponding to the chiral (piecewise chiral) regime, the sign of the Fermi velocity is independent of (depends on) μ, as illustrated in Fig. 2(a) by the dispersion of the right (chiral) and left (piecewise chiral) edge state. In the piecewise chiral regime, there is a range of μ, for which the edge states are nonchiral, i.e., there are two counterpropagating edge modes at a given boundary in contrast to the single edge mode in the chiral regime, where the velocities are opposite at opposite boundaries. In the topological phase, a nonchiral behavior is observed for μ inside the bulk gap. One can also notice the asymmetry in the localization length between the right and left edge states. For example, if $\varphi = -\pi/2$, see Fig. 2(a) [$\varphi = \pi/2$; see Fig. 2(d)], the left (right) edge state is more strongly localized than the opposite one which is consistent with Eq. (7) and the 2D finite size calculations [see Fig. 3(b)] even in the presence of disorder [see Figs. 3(b′) and 3(b″)]. The larger the gap for given k_y the more localized the edge state is.

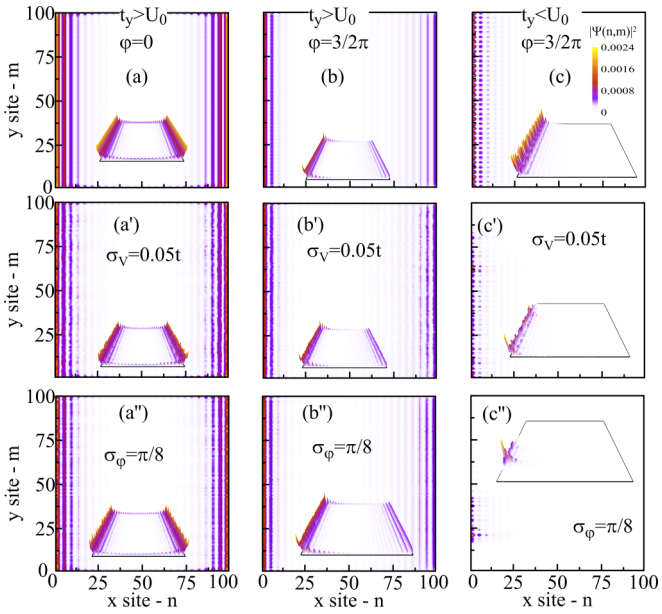

FIG. 3. Wave functions $|\Psi(n, m, E \approx 0)|^2$ of edge states for a 2D finite size lattice inside the bulk gap (near $E = 0$) in the topological phase, $t_y > U_0 = 0.05t$ for (a) $\varphi = 0$, (b) $\varphi = 3/2\pi$, and (c) in the nontopological phase, $t_y < U_0 = 0.15t$ and $\varphi = 3/2\pi$. The lower panels (a′)–(c′) and (a″)–(c″) correspond to the case of on-site disorder ($\sigma_V = 0.05t$) and disorder in the CDW phase ($\sigma_\varphi = \pi/8$). In the topological phase, the presence of edge states is not affected by weak disorder (with effective amplitude not exceeding the size of the gap), while edge states in the nontopological phase are affected by weak disorder leading to Anderson localization (around some random edge site). However, even in the latter case edge states can survive some small amount of disorder of both types when $\sigma_V \leqslant 0.1t$ and $\sigma_V \lesssim \pi/16$.

In the nontopological phase, $t_y < U_0$, the edge states exist only for particular values of the CDW phase shift φ; see Figs. 2(a″)–2(d″). Generally, there are three possible scenarios; see Fig. 4. If $t_y < -U_0 \sin\varphi$, the edge state exists inside the bulk gap without touching the bulk spectrum; see Figs. 2(a″) and 2(d″). These edge states are nonchiral and disorder, e.g., due to random impurities can result in backscattering inside the same channel, reducing the conductance. If $t_y < U_0 \sin\varphi$, the system is in the trivial phase without edge states. In the regime $U_0 > t_y > -U_0 \sin\varphi$ ($U_0 > t_y > U_0 \sin\varphi$) there are again two wave vectors $k_\pm$ at which edge states merge with

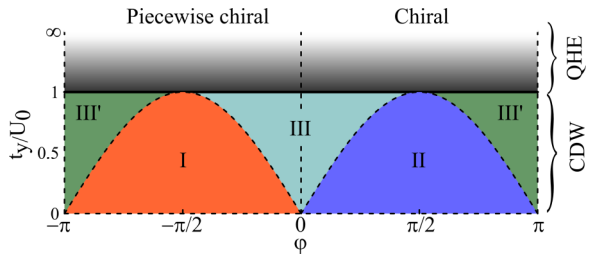

FIG. 4. Phase diagram for filling factor $\nu = 1$. If $t_y/U_0 > 1$ ($t_y/U_0 < 1$), the system is in the topological (nontopological) phase, indicated as QHE (CDW) phase. The phase transition between phases occurs at $t_y/U_0 = 1$, where the gap closes. The nontopological phase is subdivided into the following subphases: (I) (orange area) edge states are totally inside the bulk gap, (II) (blue area) no edge states, and edge states spread between two wave vectors k_- and k_+ belonging either both to the electron (III) (light green area) or both to the hole (III′) (dark green areas) band. At the phase boundary between the subphases (dashed lines), we have $k_- = k_+$. Generally, depending on the phase φ the edge states can be either chiral for all values of μ or be piecewise chiral, such that by shifting μ, opposite chiralities can be observed.

the bulk electron (hole) spectrum. As a result, there is a range of chemical potentials (corresponding to the Fermi wave vectors between k_- and k_+) for which edge states are chiral even in the nontopological phase; see Fig. 2(b″). However, these values are not in the bulk gap, so the edge states coexist with the bulk modes. The previous analysis was relying on the fact that k_y is a good quantum number in the absence of disorder. Similar to Weyl semimetals [38–43], one can expect to detect [44] such chiral edge states in a gapless bulk by searching for an enhanced response at the boundaries. Similarly, weak disorder cannot eliminate these merging points at $k_\pm$ (e.g., by combining them) as they are protected by continuity of our analytical solutions.

IV. DISORDER EFFECTS

In realistic systems one cannot avoid disorder. In our 2D finite size lattice model, we study effects of disorder by introducing (i) a random on-site potential $\sum_{n,m} V_{n,m} c^\dagger_{n,m} c_{n,m}$ and (ii) a random phase $\tilde{\varphi}_m$ for the CDW modulation in each wire, i.e., $2U_0 \sum_{n,m} \cos(2k_w n a_x + \varphi + \tilde{\varphi}_m) c^\dagger_{n,m} c_{n,m}$. Here, $V_{n,m}$ ($\tilde{\varphi}_m$) is taken according to a Gaussian distribution with zero mean and standard deviation σ_V (σ_φ). By analyzing the edge state wave functions $|\Psi(n,m,\varphi)|^2$ in different phases (see Fig. 3), we see that, for the given variance $\sigma_V \lesssim 0.1t$, the on-site disorder does not destroy the edge states in both topological [also the asymmetry in localization lengths is preserved; see Fig. 3(b′)] and nontopological phases; see Figs. 3(a′)–3(c′) [30]. Interestingly, chiral QHE edge states survive any amount of disorder in the phase φ, while in the nontopological phase, the edge states survive only up to a certain small amount of disorder σ_φ with stronger disorder leading to Anderson localization around a random location along the edge. Importantly, the magnetic field stabilizes the edge states induced by the CDW also in the nontopological regime by suppressing backscattering caused by disorder. In our numerics on finite size systems such localization effects were always negligible in the parameter regimes considered.

V. SUMMARY

We have studied a system of weakly coupled and CDW modulated wires in a perpendicular magnetic field. The system supports edge states in both the nontopological (CDW dominated) and topological (QHE dominated) phase. Interestingly, both phases host chiral and nonchiral edge states depending on the chemical potential position. Numerical calculations showed that, in general, the edge states in the nontopological phase are more affected by the disorder than in the topological phase; however, the former can still survive a finite amount of disorder. We propose that our predictions can be tested in semiconducting nanowires with CDW modulations, heterostructures [16,17], organic conductors [45], but also in optical lattices [46–48] or photonic crystals [49]. Finally, it would be interesting to see if our results can be extended to other models in 2D and 3D, which include TI phases with (piecewise) helical edge states.

ACKNOWLEDGMENTS

We acknowledge support from the Swiss NSF (SNSF), NCCR QSIT, and SCIEX.

APPENDIX A: EFFECTIVE LINEARIZED HAMILTONIAN

In the weak coupling regime $t_y, |U_0| \ll t$, when tunneling and CDW modulation can be treated as small perturbations, the continuum version of the Hamiltonian $H_x = \sum_{n,k_y}[-t c^\dagger_{n+1,k_y} c_{n,k_y} + \text{H.c.}] - \sum_{n,k_y} \mu c^\dagger_{n,k_y} c_{n,k_y}$ can be linearized in the vicinity of the Fermi points, $\pm k_F$ [29,32]. The corresponding electron annihilation operator can be expressed in terms of slowly varying left $[L(x)]$ and right movers $[R(x)]$ as

$$\Psi(x) = R(x)e^{ik_F x} + L(x)e^{-ik_F x}. \tag{A1}$$

As a result by dropping out all fast oscillating terms, we rewrite the kinetic-energy term H_x in the linearized model as

$$H_x^{\text{lin}} = i\hbar v_F \int dx \left[L^\dagger(x) \frac{\partial L(x)}{\partial x} - R^\dagger(x) \frac{\partial R(x)}{\partial x} \right], \tag{A2}$$

where v_F is the Fermi velocity. The Hamiltonian corresponding to the charge density modulation $U(x) = -2U_0 \cos(2k_w x + \varphi)$ that resonantly couples the left and the right movers for $k_w = k_F$ and can be written as

$$H^{\text{lin}}_{\text{CDW}} = -U_0 \int dx \, [e^{i\varphi} R^\dagger(x) L(x) + \text{H.c.}]. \tag{A3}$$

Here, we again neglected all fast-oscillating terms. We note that Eq. (3) can be of use also in the case if the system is slightly out of the resonance $k_w = k_F + \delta_k$ if $\hbar v_F \delta_k \ll |U_0|$. Thus the deviation can be quite substantial if the amplitude U_0 is large. However, we also note that if the CDW is generated not by gates but intrinsically by electron-electron interactions then the relation $k_w = k_F$ emerges by itself (similar to a Peierls transition): the gap opened at the Fermi energy lowers the

total energy of the system and the energy gain is maximum at $k_w = k_F$.

The magnetic field at the filling factor $\nu = 1$ results in the phase $\phi = 2k_F a_x$ for tunneling matrix elements [14,20]. Thus the tunneling Hamiltonian H_y also couples resonantly the left and the right movers,

$$H_y^{\rm lin} = -t_y \int dx\, [e^{ik_y a_y} R^\dagger(x) L(x) + \text{H.c.}]. \qquad \text{(A4)}$$

To conclude, we note that the total Hamiltonian $H_x^{\rm lin} + H_{\rm CDW}^{\rm lin} + H_y^{\rm lin}$ can be conveniently represented in terms of Pauli matrices acting on the left-right mover subspace; see Eq. (3) of the main text.

APPENDIX B: ISOTROPIC LIMIT

The continuum model we used in the main text is derived in the anisotropic regime, i.e., under the assumption of weak tunneling $t_y \ll t$. While the isotropic model with $t_y = t$ is difficult to study analytically it can be easily addressed numerically by performing exact diagonalization of the tight-binding Hamiltonian given by Eq. (2) in the main text. Also in this case we find the phase transition between the topological and nontopological phases separated by the gap closing at $t_y = U_0$ (see Fig. 5) as it was shown in the main text in the anisotropic model ($t_y \ll t$). Importantly, we again observe both chiral and nonchiral edge states in both phases.

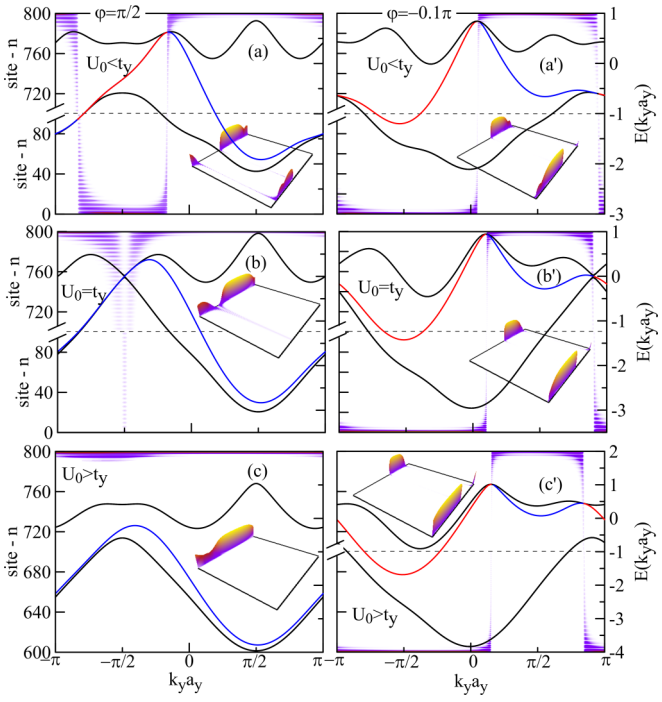

FIG. 5. Energy spectrum $E(k_y a_y)$ near the band gap at the Fermi level defined by $\mu = -\sqrt{2}t$ for the isotropic system ($t_y = t$) (a) in the topological phase ($U_0 = 0.5t$), (b) at the phase transition point ($U_0 = t$), and (c) in the nontopological phase ($U_0 = 1.5t$) found numerically. The phase of the CDW modulation is set to $\varphi = \pi/2$ [(a′), (b′), (c′) for $\varphi = -0.1\pi$]. The color map represents $|\Psi(n,k_y)|^2$ for the edge state wave function probability. The position at site n (energy) is marked on the left (right) axis. We note that edge states can be found both in the topological and nontopological phase. By changing μ, the edge states can be tuned between being chiral and nonchiral; see panels (a) and (c′).

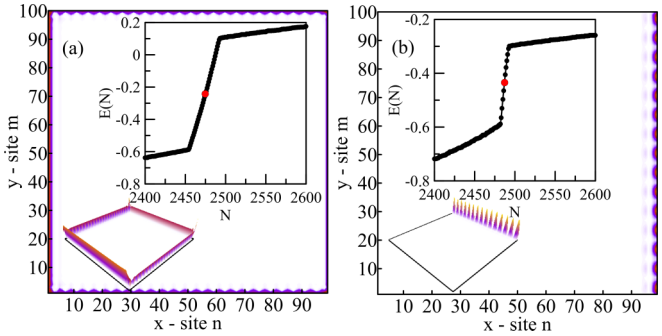

FIG. 6. Wave functions $|\Psi(n,m,E_0)|^2$ (color maps) of edge states for an isotropic ($t_y = t$) 2D finite size lattice inside the bulk gap (near the center of the gap E_0) (a) in the topological phase, $U_0 = 0.5t$, and (b) in the nontopological phase $U_0 = 1.5t$ for $\varphi = \pi/2$. The discrete energy spectrum in the gap is plotted in the insets with the corresponding state marked by the red dot. In the nontopological regime localized edge states are present only on one side of the 2D sample.

The wave functions of in-gap edge states can be also obtained by the exact diagonalization of the isotropic ($t_y = t$) 2D Hamiltonian without introducing the momentum k_y; see Fig. 6. In the topological phase, chiral edge states are present at all four sides of the 2D sample, whereas, in the nontopological phase, there are localized edge states only at one side. This difference in edge state behavior could help to distinguish between the two phases experimentally. A further possibility to distinguish the two phases is to study their robustness against disorder. In the presence of disorder, the conductance of nonchiral edges deviates from well-quantized values typical for chiral edge states.

APPENDIX C: DEPENDENCE ON THE WIDTH W OF THE STRIP

In the numerical results presented in the main text, the number of lattice sites is chosen such as to cover an integer number of Fermi wavelengths inside the strip. As a result, the discretized CDW potential has an inversion symmetry point for $\varphi = -\pi, 0, \pi$. However, one can choose the number of sites such that the length of the wire (i.e., the width W of the strip) corresponds to a half integer number of Fermi wavelengths. In this case the CDW phase shift φ at the right end of the strip is different from those in the main text; see Fig. 7. As expected, the left edge modes are not affected by this new choice, but the dispersion of the right edge mode is changed. For example, the discretized CDW potential has now an inversion symmetry point for the phase value $\varphi = 3\pi/2$. Interestingly, in the nontopological phase, $U_0 > t_y$, one can find again nonchiral edge states that do not touch the bulk modes. The 2D wave functions $|\Psi(n,m,\varepsilon \approx 0)|^2$ for both edge states present in the nontopological regime are depicted in Fig. 8.

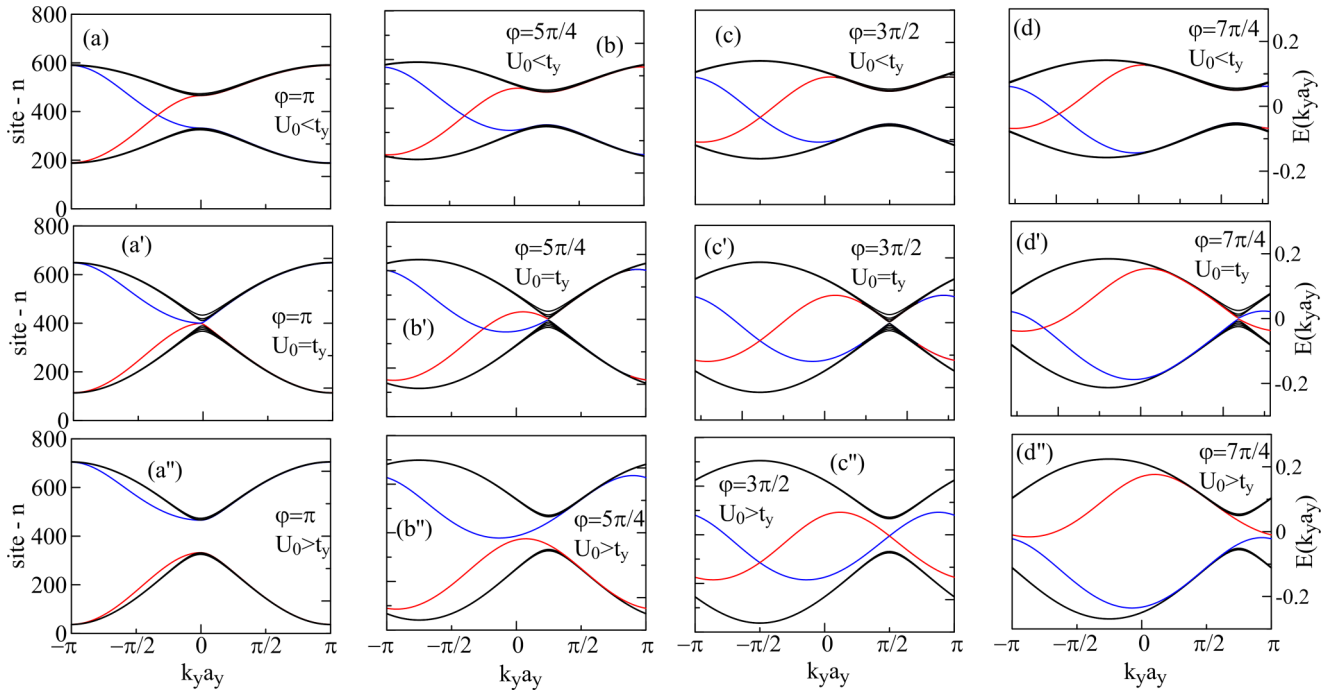

FIG. 7. Energy spectrum in the anisotropic regime ($t_y = 0.1t$) $E(k_y)$ near the band gap for the system (a)–(d) in the topological (QHE dominated) phase ($t_y > U_0 = 0.05t$), (a′)–(d′) at the phase transition point ($t_y = U_0 = 0.1t$), and (a″)–(d″) in the nontopological (CDW dominated) phase ($t_y < U_0 = 0.15t$). The panels (a), (b), (c), and (d) refer to the phase of CDW $\varphi = \pi$, $5\pi/4$, $3\pi/2$, $7\pi/4$, respectively. The spectrum of localized edge state is found numerically (dashed line) and analytically (red line). The color map represents $|\Psi(n,k_y)|^2$ for the edge state. The position, site n (energy) is marked on the left (right) axis. The found behavior of edge states is, generally, the same as described in the main text, confirming that proposed phases do not depend qualitatively on the system width.

APPENDIX D: FILLING FACTOR $\nu = 2$

One can also observe phase transitions similar to the ones described in the main text for $\nu = 1$ for the filling factor $\nu = 2$, which corresponds to an indirect resonant magnetic field with $\phi = k_F a_x$ [14,20]. In this case, the size of the gap opened by the resonant tunneling in the y direction is smaller ($\Delta \approx 2t_y^2/\mu$) than for $\nu = 1$; thus the phase transitions occur for correspondingly smaller values of U_0. In the topological phase, there are always two chiral edge states present at each edge inside the gap; see Figs. 3(a)–3(b). Interestingly, in the nontopological phase, there can be two or four modes present at the same edge; see Fig. 9(b′). Similarly to $\nu = 1$, we observe chiral and nonchiral edge states in both topological and nontopological regimes.

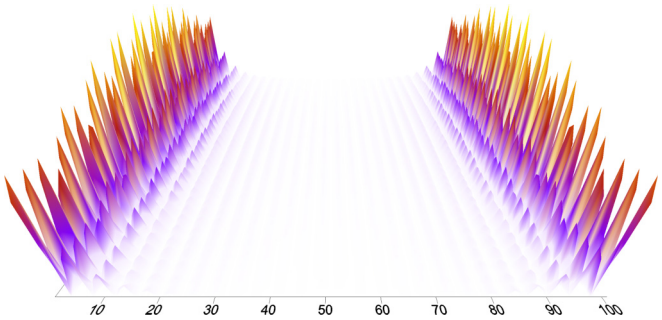

FIG. 8. Wave function $|\Psi(n,m,E \approx 0)|^2$ for the zero edge states inside the gap in the nontopological phase $|t_y| < |U_0| = 0.15t$ and $\varphi = 3/2\pi$ where both edge states are present; see Fig. 7.

APPENDIX E: CONNECTION TO 2D TIs

Mentioning of the 2D TI just served as a motivation for our work to underline the importance of studying systems that can support both topological and nontopological edge states. While the focus of our work is on QHE and CDW, we shall point out here a connection to 2D TIs and our work on a qualitative level. The spin Hall effect (present in a 2D TI) can

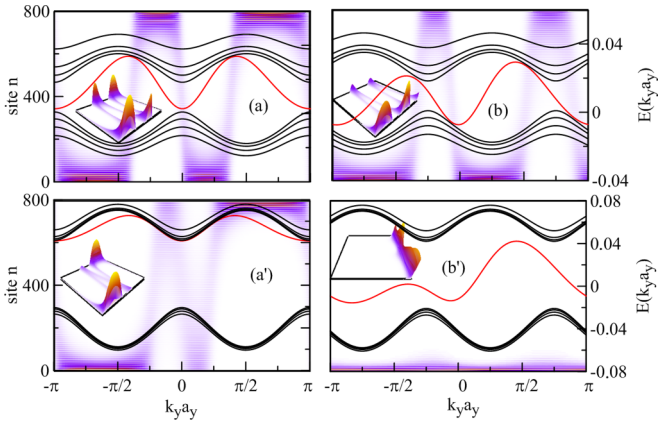

FIG. 9. Same as in Fig. 2 of the main text ($t_y = 0.1t$ and $\mu = -\sqrt{2}t$) but for the filling factor $\nu = 2$ (resulting in $\phi = k_F a_x$). (a),(b) In the topological phase ($U_0 = 0.02t$, $\varphi = 0, -\pi/2$), there are two chiral edge states present at each edge. (a′),(b′) In the nontopological phase ($U_0 = 0.1t$, $\varphi = 0, -\pi/2$), depending on the chemical potential, there could be two or four nonchiral edge states.

be considered as resulting from two uncoupled layers of spin up and spin down electrons, both in the QHE regime. Importantly, the direction of the magnetic field must then be opposite in the two layers (which models the spin-orbit interaction and preserves time reversal symmetry). Given this analogy, our study of the competition between the QHE and the CDW dominated phases can hint on the existence of similar effects also for 2D TIs, where one can address the interplay between helical and nonhelical edge states. However, explicit modeling of a 2D TI is a more subtle issue which is beyond the scope of the present work and we leave this study to future work.

In this work we focus on 2D systems. However, our ideas on coexistence of two types of edge states of course could be extended to 1D [32,50–52] and 3D systems.

[1] K. v. Klitzing, G. Dorda, and M. Pepper, Phys. Rev. Lett. **45**, 494 (1980).

[2] D. C. Tsui, H. L. Stormer, and A. C. Gossard, Phys. Rev. Lett. **48**, 1559 (1982).

[3] D. J. Thouless, M. Kohmoto, M. P. Nightingale, and M. den Nijs, Phys. Rev. Lett. **49**, 405 (1982).

[4] M. Z. Hasan and C. L. Kane, Rev. Mod. Phys. **82**, 3045 (2010).

[5] S. Hart, H. Ren, T. Wagner, P. Leubner, M. Mühlbauer, C. Brüne, H. Buhmann, L. W. Molenkamp, and A. Yacoby, Nat. Phys. **10**, 638 (2014).

[6] V. S. Pribiag, A. J. Beukman, F. Qu, M. C. Cassidy, C. Charpentier, W. Wegscheider, and L. P. Kouwenhoven, Nat. Nanotechnol. **10**, 593 (2015).

[7] E. M. Spanton, K. C. Nowack, L. Du, G. Sullivan, R.-R. Du, and K. A. Moler, Phys. Rev. Lett. **113**, 026804 (2014).

[8] Y. H. Wang, J. R. Kirtley, F. Katmis, P. Jarillo-Herrero, J. S. Moodera, and K. A. Moler, Science **349**, 948 (2015).

[9] I. Tamm, Phys. Z. Sowjetunion **1**, 733 (1932).

[10] W. Shockley, Phys. Rev. **56**, 317 (1939).

[11] S. Gangadharaiah, L. Trifunovic, and D. Loss, Phys. Rev. Lett. **108**, 136803 (2012).

[12] F. Nichele, H. J. Suominen, M. Kjaergaard, C. M. Marcus, E. Sajadi, J. A. Folk, F. Qu, A. A. J. Beukman, F. K. d. Vries, J. v. Veen, S. Nadj-Perge, L. P. Kouwenhoven, B.-M. Nguyen, A. A. Kiselev, W. Yi, M. Sokolich, M. J. Manfra, E. M. Spanton, and K. A. Moler, arXiv:1511.01728.

[13] T. Giamarchi, *Quantum Physics in One Dimension*, International Series of Monographs on Physics (Clarendon Press, Oxford, 2003).

[14] J. Klinovaja and D. Loss, Eur. Phys. J. B **87**, 171 (2014).

[15] K. S. Bedell, *Strongly Correlated Electronic Materials: The Los Alamos Symposium 1993*, edited by K. S. Bedell *et al.* (AddisonWesley, Reading, 1994), p. 15.

[16] R. E. Algra, M. A. Verheijen, M. T. Borgström, L.-F. Feiner, G. Immink, W. J. van Enckevort, E. Vlieg, and E. P. Bakkers, Nature (London) **456**, 369 (2008).

[17] R. A. Deutschmann, W. Wegscheider, M. Rother, M. Bichler, G. Abstreiter, C. Albrecht, and J. H. Smet, Phys. Rev. Lett. **86**, 1857 (2001).

[18] A. G. Lebed, Pis'ma Zh. Eksp. Teor. Fiz. **43**, 137 (1986) [JETP Lett. **43**, 174 (1986)].

[19] V. M. Yakovenko, Phys. Rev. B **43**, 11353 (1991).

[20] J. Klinovaja and D. Loss, Phys. Rev. Lett. **111**, 196401 (2013).

[21] J. C. Y. Teo and C. L. Kane, Phys. Rev. B **89**, 085101 (2014).

[22] J. Klinovaja and Y. Tserkovnyak, Phys. Rev. B **90**, 115426 (2014).

[23] I. Seroussi, E. Berg, and Y. Oreg, Phys. Rev. B **89**, 104523 (2014).

[24] E. Sagi and Y. Oreg, Phys. Rev. B **90**, 201102 (2014).

[25] T. Meng and E. Sela, Phys. Rev. B **90**, 235425 (2014).

[26] J. Klinovaja, Y. Tserkovnyak, and D. Loss, Phys. Rev. B **91**, 085426 (2015).

[27] T. Meng, T. Neupert, M. Greiter, and R. Thomale, Phys. Rev. B **91**, 241106 (2015).

[28] B. Braunecker, G. I. Japaridze, J. Klinovaja, and D. Loss, Phys. Rev. B **82**, 045127 (2010).

[29] J. Klinovaja and D. Loss, Phys. Rev. B **86**, 085408 (2012).

[30] One can set the system parameters and disorder strength in such a way that only QHE edge states will survive.

[31] J. Alicea, Rep. Prog. Phys. **75**, 076501 (2012).

[32] J. Klinovaja, P. Stano, and D. Loss, Phys. Rev. Lett. **109**, 236801 (2012).

[33] D. Rainis, L. Trifunovic, J. Klinovaja, and D. Loss, Phys. Rev. B **87**, 024515 (2013).

[34] R. Jackiw and C. Rebbi, Phys. Rev. D **13**, 3398 (1976).

[35] W. P. Su, J. R. Schrieffer, and A. J. Heeger, Phys. Rev. Lett. **42**, 1698 (1979).

[36] S. Kivelson and J. R. Schrieffer, Phys. Rev. B **25**, 6447 (1982).

[37] J. Klinovaja and D. Loss, Phys. Rev. Lett. **110**, 126402 (2013).

[38] X. Wan, A. M. Turner, A. Vishwanath, and S. Y. Savrasov, Phys. Rev. B **83**, 205101 (2011).

[39] K.-Y. Yang, Y.-M. Lu, and Y. Ran, Phys. Rev. B **84**, 075129 (2011).

[40] A. A. Burkov and L. Balents, Phys. Rev. Lett. **107**, 127205 (2011).

[41] G. Xu, H. Weng, Z. Wang, X. Dai, and Z. Fang, Phys. Rev. Lett. **107**, 186806 (2011).

[42] A. A. Zyuzin and A. A. Burkov, Phys. Rev. B **86**, 115133 (2012).

[43] J. Klinovaja, P. Stano, and D. Loss, Phys. Rev. Lett. **116**, 176401 (2016).

[44] Y. Baum, T. Posske, I. C. Fulga, B. Trauzettel, and A. Stern, Phys. Rev. Lett. **114**, 136801 (2015).

[45] K. Kobayashi, H. Satsukawa, J. Yamada, T. Terashima, and S. Uji, Phys. Rev. Lett. **112**, 116805 (2014).

[46] M. Lewenstein, A. Sanpera, V. Ahufinger, B. Damski, A. Sen, and U. Sen, Adv. Phys. **56**, 243 (2007).

[47] M. Aidelsburger, M. Atala, M. Lohse, J. T. Barreiro, B. Paredes, and I. Bloch, Phys. Rev. Lett. **111**, 185301 (2013).

[48] M. Aidelsburger, M. Lohse, C. Schweizer, M. Atala, J. T. Barreiro, S. Nascimbene, N. Cooper, I. Bloch, and N. Goldman, Nat. Phys. **11**, 162 (2015).

[49] Y. E. Kraus, Y. Lahini, Z. Ringel, M. Verbin, and O. Zilberberg, Phys. Rev. Lett. **109**, 106402 (2012).

[50] J. Klinovaja and D. Loss, Eur. Phys. J. B **88**, 1 (2015).

[51] D. Rainis, A. Saha, J. Klinovaja, L. Trifunovic, and D. Loss, Phys. Rev. Lett. **112**, 196803 (2014).

[52] T. Ojanen, Phys. Rev. B **87**, 100506 (2013).